Obtaining accurate ground-state properties on near-term quantum devices

Qi-Ming Ding,[1,2] Jiawei Peng,[3,4] Junxiang Huang,[1,2] Yukun Zhang,[1,2] Huiyuan Wang,[1,2,5] Xiaosi Xu,[6] Jiajun Ren,[7] Yingjin Ma,[4,*] and Xiao Yuan[1,2,†]

[1] *Center on Frontiers of Computing Studies, Peking University, Beijing 100871, China*
[2] *School of Computer Science, Peking University, Beijing 100871, China*
[3] *MOE Key Laboratory of Environmental Theoretical Chemistry, South China Normal University, Guangzhou 510006, China*
[4] *Computer Network Information Center, Chinese Academy of Sciences, Beijing 100190, China*
[5] *Peterhouse, Univeristy of Cambridge, Cambridge CB2 1RD, United Kingdom*
[6] *Graduate School of China Academy of Engineering Physics, Beijing 100193, China*
[7] *Key Laboratory of Theoretical and Computational Photochemistry, Ministry of Education, College of Chemistry, Beijing Normal University, Beijing 100875, China*

(Received 20 October 2025; revised 5 January 2026; accepted 3 April 2026; published 21 May 2026)

Accurate ground-state calculations on noisy quantum computers are significantly constrained by restricted *Ansatz* expressivity and unavoidable hardware errors. We introduce a hybrid quantum-classical framework that simultaneously addresses these challenges. Our method systematically purifies noisy two-electron reduced density matrices from quantum devices by enforcing N-representability conditions through efficient semidefinite programming, guided by a norm-based distance constraint to the experimental data. To implement this constraint, we develop a hardware-efficient calibration protocol based on Clifford circuits. We demonstrate near full configuration-interaction accuracy for ground-state energies of H_2, LiH, and H_4, and compute precise scattering intensities for C_6H_8 on noisy hardware. This approach surpasses conventional methods by simultaneously overcoming both *Ansatz* limitations and hardware noise, providing a framework for quantum advantage and offering an alternative for reliable simulations of complex molecular systems on noisy devices.

DOI: 10.1103/lx3w-w6jx

I. INTRODUCTION

Predicting the behavior of quantum many-body systems is a fundamental challenge that underpins key developments across science and technology [1], from understanding low-energy phases of matter [2] and designing novel catalysts [3] to elucidating the mechanisms of high-temperature superconductivity [4]. Tackling this challenge is limited by the exponential scaling of the Hilbert space, a "curse of dimensionality" that prohibits exact solutions of the Schrödinger equation for all but the smallest systems. This has spurred the development of powerful approximation strategies. One path, guided by the Rayleigh-Ritz variational principle [5,6], seeks an *upper* bound to the ground-state energy via a wave function *Ansatz*. The emergence of quantum computing has revitalized this principle, most notably through the variational quantum eigensolver (VQE) and related variational quantum algorithms [7–10]. Recent theoretical and experimental progress [11–15] has demonstrated that these methods can enable efficient and accurate determination of ground-state properties for systems beyond the reach of classical computation.

However, the practical implementation of the VQE on current noisy intermediate-scale quantum (NISQ) devices [16] faces critical obstacles, most notably the restricted depth of quantum circuits and the prevalence of hardware noise. On the one hand, the absence of quantum error correction confines NISQ hardware to shallow circuits, severely limiting the expressive power of quantum *Ansätze*. On the other hand, gate infidelities, decoherence, and measurement errors not only degrade accuracy but can also produce unphysical quantum states. As a result, pioneering experimental demonstrations have thus far been limited to small molecular systems [11–13], while extending these methods to larger and chemically realistic problems on practical NISQ hardware remains an outstanding challenge.

Here, we introduce a framework that extends beyond conventional hybrid quantum-classical algorithms [8] and error-mitigation techniques [17–19] by simultaneously

*Contact author: yingjin.ma@sccas.cn
†Contact author: xiaoyuan@pku.edu.cn

addressing these two central limitations. By enforcing N-representability constraints [20–23] through classical postprocessing of raw quantum data, our approach effectively amplifies circuit expressivity while mitigating the noise during the computation and measurement. A norm-based distance between corrected and measured two-electron reduced density matrices (2-RDMs), calibrated via a hardware-efficient Clifford protocol, provides a systematic and scalable route to robust accuracy. This framework consistently achieves near full configuration-interaction (FCI) accuracy for molecular ground-state energies, including H_2, LiH, and H_4, and even surpasses the accuracy of the ideal noiseless VQE by overcoming *Ansatz* limitations. Extending beyond energetics, we further demonstrate its versatility by reproducing ultrafast electron diffraction (UED) intensities of C_6H_8 with high fidelity. Together, these results establish a versatile framework for reliable quantum chemistry computation on NISQ devices, demonstrating a feasible approach toward practical quantum advantage in chemistry and materials science.

II. PRELIMINARIES

A. The electronic Hamiltonian and reduced density matrices

The Hamiltonian of a molecule after the Born-Oppenheimer approximation and second quantization can be expressed as

$$H = \sum_{ij} h_j^i a_i^\dagger a_j + \sum_{pqrs} V_{rs}^{pq} a_p^\dagger a_q^\dagger a_r a_s + H_n, \tag{1}$$

where $a^\dagger$ (a) denotes the creation (annihilation) operators of the spin orbitals, h_j^i and V_{rs}^{pq} the one- and two-electron interactions, and H_n collects all nonelectron effects such as the interaction between the nuclei. The energy of a state $|\psi\rangle$ with respect to this system is given by the expectation value of the Hamiltonian (1),

$$E = \langle\psi|H|\psi\rangle = \sum_{ij} h_j^i \langle a_i^\dagger a_j\rangle + \sum_{pqrs} V_{rs}^{pq} \langle a_p^\dagger a_q^\dagger a_r a_s\rangle + H_n \tag{2}$$

$$= \sum_{ij} h_j^i D_j^i + \sum_{pqrs} V_{rs}^{pq} D_{rs}^{pq} + H_n, \tag{3}$$

where we have introduced $\langle\cdot\rangle = \langle\psi|\cdot|\psi\rangle$ as shorthand notation and D_j^i and D_{rs}^{pq} are the one- and two-electron RDMs [20] for a quantum state $|\psi\rangle$, defined as

$$D_j^i = \langle\psi|a_i^\dagger a_j|\psi\rangle,\ D_{rs}^{pq} = \langle\psi|a_p^\dagger a_q^\dagger a_s a_r|\psi\rangle. \tag{4}$$

Measuring these RDM elements to the additive error ϵ generally requires $\Omega(N^k/\epsilon^2)$ independent state preparations for a k-body RDM on an N-orbital system [24]. In practice, one can partition the corresponding Pauli operators into mutually commuting groups, so that all terms within each group are estimated simultaneously, thereby reducing the total number of measurement settings.

B. The variational quantum eigensolver

As a hybrid quantum-classical approach, the VQE leverages the Rayleigh-Ritz variational principle [5,6,25] to optimize the lowest possible expectation energy of a trial wave function,

$$E_0 = \min_{\boldsymbol{\theta}} \langle\psi(\boldsymbol{\theta})|H|\psi(\boldsymbol{\theta})\rangle, \tag{5}$$

where the $\boldsymbol{\theta} = \{\theta_1, \theta_2, \ldots\}$ denotes a set of variational parameters of the quantum circuit, serving as an approximation to the ground-state energy of a quantum system. On the one hand, one needs a deep quantum circuit to increase the expressive power of the parametrized state $|\psi(\boldsymbol{\theta})\rangle$. However, the presence of quantum noise means that even with a highly expressive *Ansatz*, the experimentally measured 2-RDM, denoted $(D_{rs}^{pq})_{\text{noisy}}$, is noisy and unreliable. Its elements, estimated via Pauli measurements on the quantum device, are not guaranteed to correspond to a physical state and may violate the standard N-representability conditions.

C. Variational 2-RDM method and N-representability

The challenge of unphysical RDMs can be addressed by projecting the noisy data onto the set of valid RDMs. This concept is central to the classical variational 2-RDM (v2RDM) method [20–23], which enforces N-representability conditions [26–29] within a semidefinite program. Although the v2RDM method provides only a deterministic *lower* bound to the ground-state energy [30–32], it has been extensively applied across diverse scientific fields, from chemistry and materials science [33–36], quantum phase transitions [37,38], electron-nuclei coupling [22,39–42], and molecular conductance [43,44] to high-temperature superconductivity [45]. More recently, it has also emerged as a versatile approach in quantum computing [15,46–51].

The N-representability conditions ensure that an RDM corresponds to a valid physical N-particle state. A computationally tractable and widely used subset of these conditions is the DQG conditions, which impose positive semidefiniteness constraints on the two-electron (D), two-hole (Q), and particle-hole (G) matrices. The elements of these matrices are defined as follows:

$$D_{rs}^{pq} = \langle\psi|a_p^\dagger a_q^\dagger a_r a_s|\psi\rangle, \tag{6a}$$

$$Q_{pq}^{rs} = \langle\psi|a_p a_q a_r^\dagger a_s^\dagger|\psi\rangle, \tag{6b}$$

$$G_{qs}^{pr} = \langle\psi|a_p^\dagger a_q a_r^\dagger a_s|\psi\rangle. \tag{6c}$$

Enforcing these conditions, along with other constraints like Hermiticity, antisymmetry, and trace normalization, defines the set of DQG-feasible RDMs. The full set of constraints is as follows:

$$D^{pq}_{rs} = (D^{rs}_{pq})^*, \tag{7a}$$

$$D^{pq}_{rs} = -D^{pq}_{sr} = -D^{qp}_{rs} = D^{qp}_{sr}, \tag{7b}$$

$$\sum_i D^i_i = n, \ \sum_{pq} {}^2D^{pq}_{pq} = n(n-1), \tag{7c}$$

$$D^i_j = \frac{1}{N-1} \sum_k {}^2D^{ik}_{jk}, \tag{7d}$$

$$D \succeq 0, \quad Q \succeq 0, \quad G \succeq 0. \tag{7e}$$

It is crucial to note that using such a subset is a practical necessity, as the full N-representability problem is known to be QMA-complete [52]. This implies it cannot be fully characterized by a polynomial number of constraints (under the assumption of QMA $\neq P$), where, in computational complexity, P denotes the class of problems that are efficiently solvable by a classical computer in polynomial time. Conversely, QMA (Quantum Merlin Arthur) serves as the quantum analogue of NP, characterizing problems for which a proposed solution can be efficiently verified by a quantum computer given an appropriate quantum state as a proof. While stronger approximations like the $T1$ and $T2$ conditions exist [28,53], the DQG conditions offer a robust and computationally tractable approach. Indeed, enforcing them scales polynomially with the number of orbitals r, requiring $O(r^4)$ memory and $O(r^6)$ floating-point operations.

III. FRAMEWORK

A. Distance-constrained RDM correction framework

To address the issue of noisy RDMs from VQE experiments, a constrained optimization framework is introduced, as illustrated in Fig. 1. This method employs classical postprocessing to refine the initial quantum data. Our approach extends prior RDM correction schemes that primarily project an unphysical state onto the set of N-representable matrices [15,46,54]. Beyond ensuring physicality, we introduce a controlled search within a defined vicinity of the reference data to systematically seek a lower energy. This leads to the following constrained optimization problem:

$$\begin{aligned} &\underset{D^{pq}_{rs}}{\text{minimize}} \quad \mathrm{Tr}\left(K^{pq}_{rs} D^{pq}_{rs}\right), \\ &\text{subject to} \quad N\text{-representability conditions [Eqs. (7a)-(7e)]}, \\ &\qquad \left\| D^{pq}_{rs} - (D^{pq}_{rs})_{\text{noisy}} \right\|_F \leq \Delta. \end{aligned} \tag{8}$$

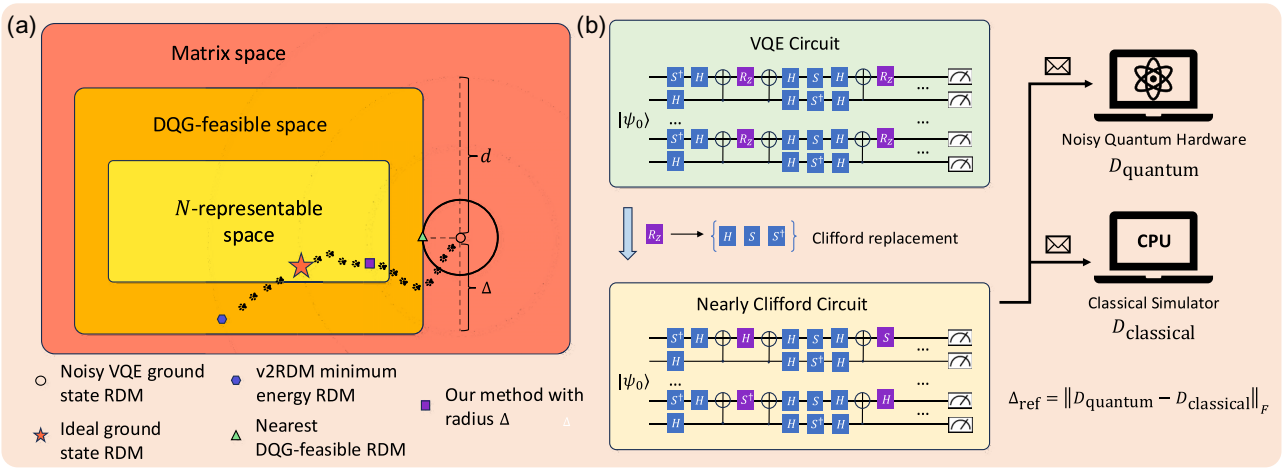

FIG. 1. Schematic of the noise-aware reduced density matrix (RDM) correction framework. (a) A conceptual diagram of RDMs in matrix space. A noisy variational quantum eigensolver (VQE) experiment yields an unphysical RDM (hollow circle), which lies at a theoretical (but unknown) distance d from the ideal ground-state RDM (red star). Our method (purple square) corrects this by finding an RDM that is DQG-feasible (within the orange space) and is constrained to a trust radius Δ around the noisy result. As shown by the optimization path (paw prints), this process yields a purified RDM that resides within the physical N-representable space (yellow). This approach is contrasted with other points like the nearest DQG-feasible RDM (green triangle) and the unconstrained variational two-electron RDM (v2RDM) global minimum (blue hexagon). The concentric circles with the hollow circle as the center represent the search results at different search radii R. The correction is most effective when the radius Δ is comparable with the error distance d. (b) The procedure to estimate the unknown error distance d and thus determine an appropriate trust radius Δ. A VQE circuit is first transformed into a "nearly Clifford circuit," which is then executed on both the noisy quantum hardware (D_{quantum}) and an ideal classical simulator ($D_{\text{classical}}$). The resulting discrepancy, $\Delta_{\text{ref}} = \|D_{\text{quantum}} - D_{\text{classical}}\|$, provides a measurable proxy for the true RDM error. This practical estimate of d then guides the selection of the trust radius Δ for the correction process on the left, ensuring an optimal correction.

Here, the objective function is the energy, where K_{rs}^{pq} is the second-order reduced Hamiltonian [21], and $\|\cdot\|_F$ denotes the Frobenius norm. The key feature of this formulation is the distance constraint, which defines a trust region of radius Δ around the initial VQE data. This constraint ensures the corrected RDM remains consistent with the original quantum state while satisfying the necessary theoretical conditions. For clarity, we refer to this method as the VQE+v2RDM framework.

The role of the trust radius Δ is central to this framework. In the limit of $\Delta \to \infty$, the distance constraint is effectively removed, and the problem reduces to a standard v2RDM calculation, which provides a lower bound to the ground-state energy. Conversely, an excessively small Δ may exclude all physically valid RDMs, making the problem infeasible. A primary task is therefore to establish an appropriate value for Δ that balances physicality and accuracy. We demonstrate the impact of this parameter in Sec. IV A using the LiH molecule as a numerical example.

B. Practical determination of the trust radius Δ

A feasible approach to determining a physically meaningful value for Δ is through theoretical derivation based on assumed noise models. In this context, the depolarizing noise model serves as a natural starting point, as it is one of the most prevalent noise sources in quantum information and represents the primary impact of environmental decoherence on quantum hardware. We have developed two such theoretical bounds, the formal derivations of which are provided in the Appendix. However, the practical utility of these theoretical bounds is limited for two primary reasons. First, simplified noise models like the depolarizing channel often fail to capture the full complexity of noise in real devices, such as thermal relaxation and nonunital coherent errors. Second, as our numerical results will demonstrate, these theoretical bounds tend to be overly conservative, yielding a conservative estimate of Δ. An excessively large trust region allows the optimization to undershoot the true ground-state energy, thereby potentially leading to suboptimal error mitigation.

To accurately estimate the deviation between the noisy VQE RDM and the ideal FCI RDM, we propose a calibration strategy using a surrogate Clifford circuit. The core of this strategy is to replace the original VQE *Ansatz* with a classically simulable proxy that preserves the hardware noise profile.

This approach is underpinned by two key observations. First, error accumulation in NISQ devices is primarily dictated by two-qubit gates. For example, the unitary coupled cluster with singles and doubles (UCCSD) *Ansatz* for H_2 is typically realized via a quantum circuit consisting of 56 CNOT gates, supplemented by 72 Hadamard, 24 S, and 32 R_z gates. Since two-qubit gate error rates are typically an order of magnitude higher than those of single-qubit gates, the noise profile is dominated by the fixed CNOT structure rather than the variable rotations. Thus, substituting rotation gates with their nearest Clifford equivalents preserves the global geometric deviation induced by noise while enabling efficient classical simulation.

The strategy of constructing reference circuits through gate substitution or simplification has been explored in recent studies. For instance, the noise-estimation approach by Urbanek *et al.* constructs simplified circuits by removing single-qubit gates to derive a global scalar rate for multiplicative correction [55]. In parallel, the method used by Farrell *et al.* executes reference circuits with variational parameters set to zero to compute a decoherence factor for observable renormalization [56]. In contrast to these approaches that focus on scalar rescaling, our calibration strategy replaces the original *Ansatz* with a surrogate Clifford circuit to estimate the global geometric deviation caused by noise.

The specific implementation of our calibration protocol is outlined as follows. First, we construct the reference circuit by systematically approximating the VQE *Ansatz*. Each non-Clifford single-qubit rotation is replaced by the candidate gate from the set $\mathcal{C} = \{H, X, Y, Z, S, S^\dagger, I\}$ that maximizes the process fidelity with the original operator. This mapping preserves the exact circuit topology and CNOT connectivity. According to the Gottesman-Knill theorem [57], such Clifford circuits generate stabilizer states that can be efficiently simulated classically in polynomial time. Consequently, the ideal reference, $(D_{rs}^{pq})_{\text{CR thm}}$, is computed exactly via classical simulation, while the noisy reference, $(D_{rs}^{pq})_{\text{CR noisy}}$, is obtained by executing the circuit on quantum hardware. Finally, we quantify the hardware-specific noise baseline, Δ_{ref}, as the Frobenius norm of the deviation between these two RDMs,

$$\Delta_{\text{ref}} = \left\| (D_{rs}^{pq})_{\text{CR thm}} - (D_{rs}^{pq})_{\text{CR noisy}} \right\|_F . \tag{9}$$

While Δ_{ref} provides a hardware-efficient estimate of the noise baseline, it primarily characterizes the hardware errors encountered by the Clifford reference circuit. To determine the total trust radius Δ, two additional sources of uncertainty must be considered. The first is the substitution discrepancy, which occurs because the noise sensitivity of the original non-Clifford gates may differ from that of their Clifford surrogates. The second is the *Ansatz* approximation error, representing the intrinsic deviation of the noiseless *Ansatz* wave function from the exact FCI ground state.

To account for these factors, the effective trust radius is defined as $\Delta = k\Delta_{\text{ref}}$, where k is a scaling factor. For a highly expressible *Ansatz* like UCCSD [7,58], k should ideally be close to 1 if the *Ansatz* is near perfect, but must be slightly larger to ensure the trust region encompasses the physical ground state. In this work, we employ $k = 2$ as a consistent heuristic. This choice balances the high

expressibility of the UCCSD *Ansatz* against the inherent hardware noise, ensuring a feasible trust region without the need for extensive hyperparameter tuning or machine-learning-based optimization, which we defer to future research.

IV. NUMERICAL SIMULATION

A. The role of the trust radius Δ

We begin by demonstrating the effect of the trust radius Δ on the calculated ground-state energy of the LiH molecule with the STO-3G basis set, which is the minimal basis set commonly used in quantum computational chemistry, at an interatomic distance of 2.8 Å. To establish clear benchmarks, we first compute the energy using three reference methods: FCI for the exact value, and both noiseless and noisy VQE calculations. The VQE simulations are performed using a UCCSD *Ansatz*, employing an active space of three orbitals that are mapped to six qubits. For the noisy simulations, we incorporate depolarizing error rates of $p_1 = 0.001$ for single-qubit gates and $p_2 = 0.01$ for two-qubit gates. Unless otherwise noted, all numerical examples in this work utilize this specific UCCSD *Ansatz* and noise model. With these reference points, we apply our method, as defined in Eq. (8), to the noisy VQE results. The outcomes, depicted in Fig. 2, show a clear and systematic trend. As Δ is increased across a wide range from 10^{-2} to 10^4, the resulting energy progressively decreases from the noisy VQE value. The corrected energy is observed to cross the FCI benchmark line and ultimately converges toward the v2RDM lower bound, demonstrating the behavior of the framework. While we observe that the v2RDM lower bound closely aligns with the FCI reference in this specific LiH instance, we emphasize that this tight agreement is not typical for all systems. In general, v2RDM minimization yields an energy strictly lower than the FCI value with a discernible gap, as documented in the literature [21]. The benchmark FCI energies, serving as our "benchmark reference," were obtained using the FCI module in PYSCF [59,60].

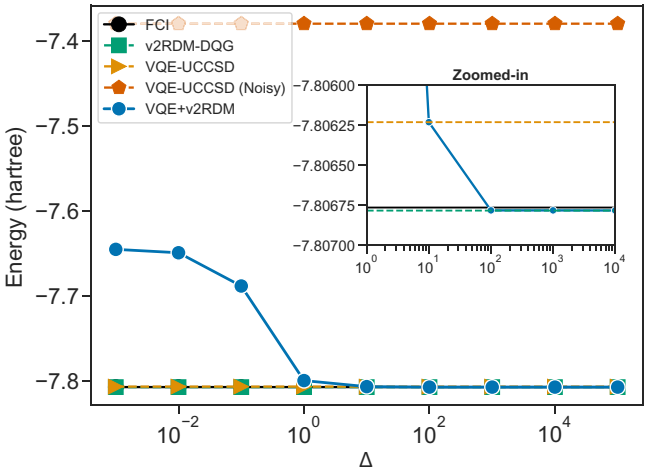

FIG. 2. Ground-state energy of the LiH molecule at an interatomic distance of $d = 2.8$ Å. The energy calculated with our variational quantum eigensolver with variational reduced density matrix (VQE + v2RDM) method shown in Eq. (8) is plotted (solid blue line with markers) as a function of the penalty coefficient Δ defined in Eq. (8). For comparison, horizontal lines indicate the benchmark full configuration-interaction (FCI) energy (solid black), the noisy result of energy from a VQE–unitary coupled cluster with singles and doubles (UCCSD) circuit (dashed orange) with error rates of $p_1 = 0.001$ for single-qubit gates and $p_2 = 0.01$ for two-qubit gates, and the result from the two-electron vRDM (v2RDM) method with DQG conditions (dashed green). The energy of VQE + v2RDM theory converges to the FCI value for large Δ. Inset: A magnified view of the converged energy region.

B. Molecular dissociation energy simulation with a classical simulator

Modeling molecular dissociation provides a rigorous benchmark for any electronic structure method because the nature of electron correlation shifts dramatically along the reaction coordinate. Near equilibrium geometry, the predominant effect is dynamic correlation, which accounts for instantaneous electron repulsion. As the bond stretches towards dissociation, however, static correlation arising from near-degenerate electronic states becomes critical, and the intermediate region exhibits a complex interplay of both. Accurately representing this transformation is a well-known challenge for a quantum *Ansatz*, whose expressive power is often limited by circuit depth and connectivity on NISQ devices. The results presented in this section demonstrate that our correction framework effectively compensates for these limitations, delivering chemically accurate energies across the entire potential energy curves (PECs).

We demonstrate our framework by calculating the dissociation curve for the H_2, LiH, and linear H_4 molecules, with results benchmarked against exact FCI calculations. For these calculations, we employed the STO-3G basis set. For H_2 and linear H_4, all orbitals and electrons (two and four electrons, respectively) were included, corresponding to simulations on four and eight qubits, respectively. For LiH, an active space of three orbitals with two active electrons was selected, resulting in a six-qubit computation.

To provide a systematic and physically motivated benchmark for our framework, we utilized the standard UCCSD *Ansatz*. However, we acknowledge that more resource-efficient strategies are highly relevant for near-term applications. Adaptive methods such as ADAPT-VQE [61], along with more efficient fermion-to-qubit encodings [62,63] and symmetry-based qubit reduction techniques [64], can significantly decrease circuit depth and qubit counts. Importantly, our v2RDM-based error mitigation framework is strictly *Ansatz*-agnostic and can

TABLE I. Comparison of Δ_{ref} and Δ_{true} for H_2, LiH, and H_4 systems across bond distances d under depolarizing noise.

	H_2		LiH		H_4	
d (Å)	Δ_{ref}	Δ_{true}	Δ_{ref}	Δ_{true}	Δ_{ref}	Δ_{true}
0.4	0.776	0.930	1.797	2.010	2.985	2.985
0.5	0.784	0.762	2.049	1.862	2.228	3.448
0.6	0.715	0.745	1.646	1.909	3.570	4.325
0.7	0.761	1.440	1.639	1.821	2.283	3.539
0.8	0.778	0.698	1.639	2.047	4.244	4.347
0.9	0.771	0.780	1.618	1.966	2.579	2.637
1.0	0.713	0.797	1.652	2.067	2.390	3.642
1.1	0.714	0.681	1.685	2.041	4.092	4.338
1.2	0.704	0.804	1.557	2.092	3.834	4.290
1.3	0.720	0.784	1.666	2.096	4.296	4.361
1.6	0.727	0.711	1.634	1.947	3.729	4.134
1.9	0.730	0.776	1.619	1.864	2.206	2.695
2.2	0.728	0.873	1.642	2.029	4.186	4.349
2.5	0.730	0.831	1.617	2.075	2.211	3.201
2.8	0.715	0.752	1.718	2.006	4.131	4.352
3.1	0.748	0.734	1.738	1.987	3.978	4.343
3.4	0.731	0.740	1.850	2.083	4.276	4.362

be seamlessly integrated with any of these resource-efficient *Ansätze* to further enhance simulation accuracy on near-term hardware.

For noiseless simulations, our primary results were obtained using the L-BFGS-B optimizer [65]; however, we also tested the COBYLA optimizer [66] and confirmed that both methods achieved chemical accuracy. To simulate realistic experimental conditions, we introduced a depolarizing noise model with single-qubit and two-qubit gate error rates of $p_1 = 0.001$ and $p_2 = 0.01$, respectively, reflecting the performance levels of current quantum hardware. In these noisy simulations, we employed the SPSA optimizer [67] with a maximum of 1000 iterations and 8192 measurement shots per observable. To mitigate the effects of stochastic fluctuations, the final energy for each point was calculated by averaging the results of the final ten optimization iterations.

The performance of our framework is illustrated in Fig. 4, which displays the potential energy curves and corresponding absolute errors for H_2, LiH, and linear H_4 molecules. For all calculations, we consistently set the expansion order to $k = 2$ to account for the unestimable error components discussed previously. To further substantiate the validity of this setting, we provide a numerical analysis of our proposed Δ_{ref} term—introduced to replace Clifford-based components—alongside the Frobenius norm of the 2-RDM difference between noisy VQE and FCI results, denoted as Δ_{true}. These results are summarized in Table I, which presents a detailed comparison across various internuclear distances for all three molecular systems. Notably, for most distances, Δ_{true} is found to be larger than Δ_{ref} but remains well within twice its value, i.e., $\Delta_{\text{ref}} < \Delta_{\text{true}} < 2\Delta_{\text{ref}}$. This numerical evidence

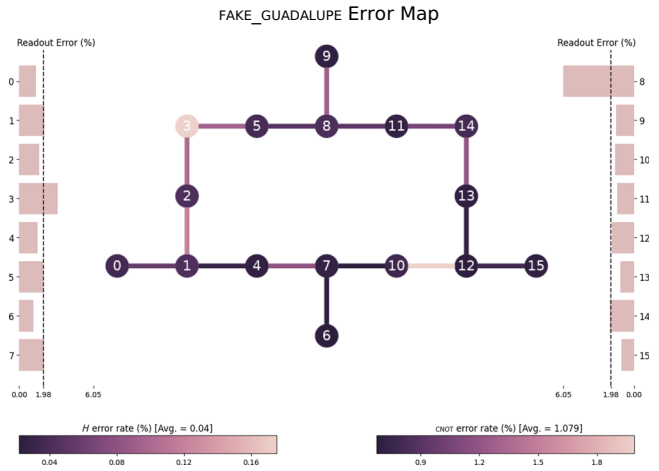

FIG. 3. Topology and error characteristics of the FAKE_GUADALUPE quantum processor. The map illustrates the connectivity of 16 physical qubits, where node colors indicate the error rates of single-qubit gates and edge colors represent two-qubit gate error rates. The horizontal bar charts on the left and right display the readout error percentages for each individual qubit. These device-specific noise parameters are integrated into the FAKEGUADALUPEV2 backend to provide a realistic hardware environment for the noisy variational quantum eigensolver (VQE) simulations.

confirms that setting $k = 2$ is a reasonable and sufficient choice for the molecular systems and error scales considered in this work.

With the validity of our error-compensation parameter established, the resulting error mitigation performance is robust. As shown in the absolute error plots (bottom row of Fig. 4), the ideal noiseless VQE-UCCSD results for the H_2 molecule achieve a precision of approximately 10^{-11} hartree, achieving a precision well below the chemical accuracy threshold. In contrast, the errors for the traditional v2RDM-DQG method and our corrected results plateau near 10^{-7} to 10^{-6} hartree, a behavior that aligns with the convergence tolerance of the SDP solver using CVXPY [68]. For the more complex LiH and linear H_4 systems, the impact of hardware-proximal noise is evident, with uncorrected VQE results (blue dashed lines) deviating significantly from the FCI benchmark. However, our proposed framework demonstrates its effectiveness by restoring the noisy VQE results to within the chemical accuracy threshold, 1.6×10^{-3} hartree, across the entire dissociation coordinate. This performance indicates the effectiveness of the proposed framework to effectively compensate for both stochastic and systematic errors in a noisy quantum environment.

C. Molecular dissociation energies simulation with IBM fake backend

To evaluate the robustness of our framework under realistic hardware constraints, we performed noisy numerical

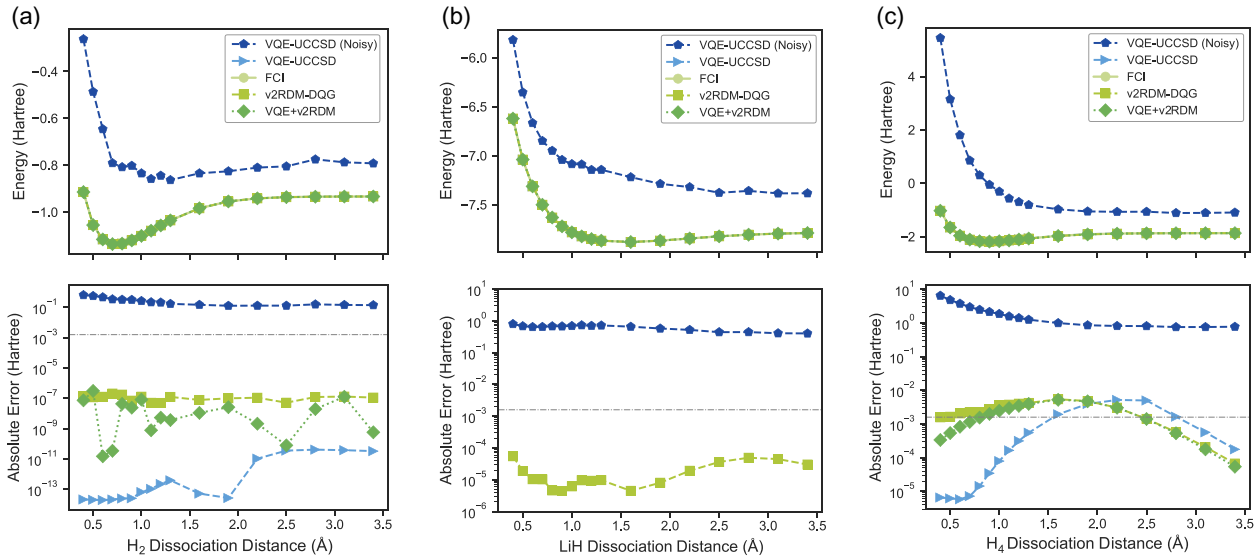

FIG. 4. Potential energy curves and errors with FCI for the dissociation of (a) the H_2, (b) the LiH, and (c) a linear H_4 molecule using the UCCSD *Ansatz* with simulated depolarizating noise. The noisy simulations assume a depolarizing channel with single- and two-qubit gate error probabilities of $p_1 = 0.001$ and $p_2 = 0.01$, respectively. In all plots, results from noisy VQE calculations (dark blue pentagons) are compared against the exact FCI benchmark (light green circles), ideal noiseless VQE simulations (light blue triangles), results obtained from the variational two-particle reduced density matrix method subject to the D, Q, and G conditions (v2RDM-DQG, yellow-green squares), and our VQE+v2RDM method (dark green rhombi). The dash-dotted line at 1.6×10^{-3} hartree marks the chemical accuracy threshold.

simulations using the FAKEGUADALUPEV2 backend from the IBM Quantum fake provider module. This backend is designed to emulate the physical behavior of the IBM Guadalupe system by utilizing system snapshots, which include critical parameters such as coupling maps, basis gates, and qubit properties, e.g., T_1, T_2, and gate error rates. The device topology and characteristic noise distribution of the FAKE_GUADALUPE processor are illustrated in Fig. 3, where the average single-qubit gate error rate is 0.04% and the average two-qubit gate error rate is 1.079%. For each

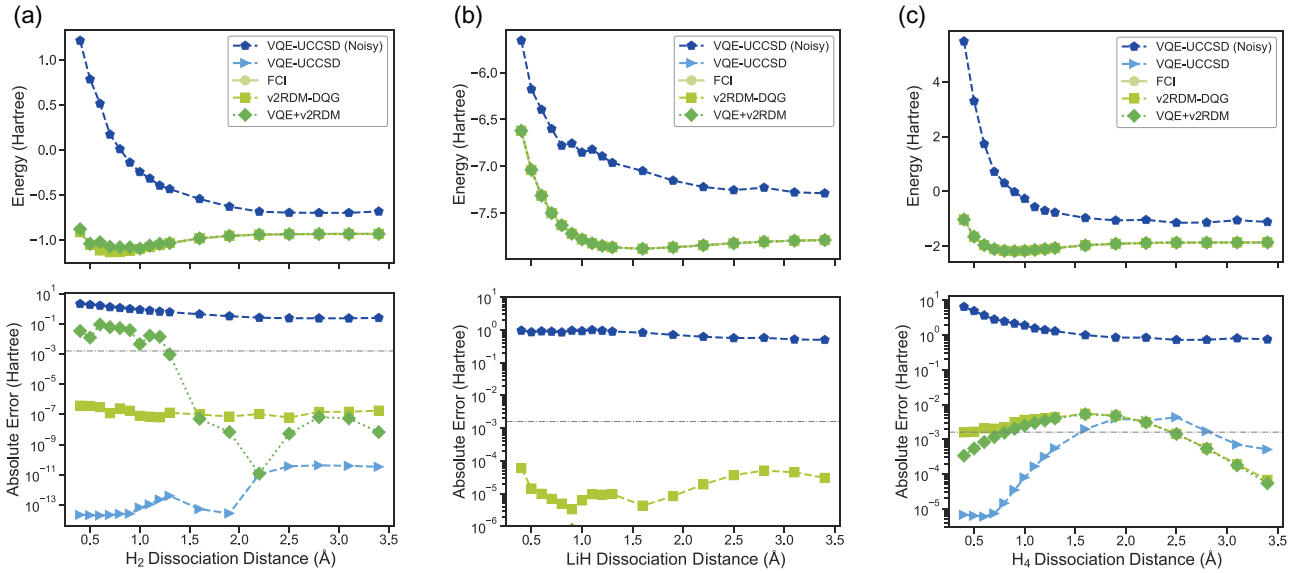

FIG. 5. Potential energy curves and errors with FCI for the dissociation of (a) the H_2, (b) the LiH, and (c) a linear H_4 molecule using the UCCSD *Ansatz* with the IBM fake backend. In all plots, results from noisy VQE calculations (dark blue pentagons) are compared against the exact FCI benchmark (light green circles), ideal noiseless VQE simulations (light blue triangles), results obtained from the variational two-particle reduced density matrix method subject to the D, Q, and G conditions (v2RDM-DQG, yellowgreen squares), and our VQE + v2RDM method (dark green rhombi). The dashdotted line at 1.6×10^{-3} hartree marks the chemical accuracy threshold.

molecular system, the specific physical qubits were automatically assigned by the Qiskit transpiler. This mapping process optimizes the simulation by selecting the most suitable qubit subset based on real-time connectivity and minimizing the cumulative impact of readout and gate errors across the required circuit topology.

To further evaluate the framework under realistic conditions, we performed simulations using the FAKE_GUADALUPE backend. The error rates for this backend are depicted in the bottom row of Fig. 3. As illustrated by the simulation results in Fig. 5, our scheme consistently demonstrates robust error mitigation capabilities, outperforming the uncorrected VQE results across the studied configurations. However, for the H_2 molecule at small internuclear distances, the absolute error with the current setting of $k = 2$ remains slightly above the chemical accuracy threshold. To understand this behavior, we must examine the interplay between the potential energy surface (PES) topology and our noise-estimation protocol. At larger distances (> 2 Å), the system exhibits a strong multireference character; our enforced DQG conditions effectively capture this static correlation, resulting in highly accurate energy recovery. In contrast, at short distances near the repulsive wall, the PES is exceedingly steep. In this highly compressed regime, the residual error stems from a "substitution discrepancy" in our Clifford-based calibration. Specifically, the Clifford surrogates cannot perfectly reproduce the complex, asymmetric hardware noise (e.g., amplitude damping and readout biases) inherent to the FAKE_GUADALUPE backend. This discrepancy causes the directionally distorted measured RDM to occasionally exceed the conservative $k = 2$ trust radius. When multiplied by the massive Hamiltonian elements at short distances, even marginal out-of-bound deviations result in disproportionate energy penalties.

While the numerical analysis in Table I confirms that $k = 2$ is sufficient to bound isotropic depolarizing noise, accommodating the realistic, structured noise of the FAKE_GUADALUPE snapshot near the steep repulsive wall requires a more forgiving boundary. As illustrated in Fig. 6, we specifically expanded the trust radius to $k = 3$ for the short-distance regime (< 2 Å) of the H_2 potential energy surface. This targeted adjustment effectively absorbs the substitution discrepancy and higher-order systematic biases. Notably, in this compressed region, the $k = 3$ configuration outperforms both the unmitigated noisy UCCSD simulations and the baseline VQE + v2RDM ($k = 2$) results, successfully restoring the energy to within chemical accuracy. Nevertheless, even with the conservative $k = 2$ setting, the proposed framework provides robust corrections for the rest of the H_2 curve, as well as the more complex LiH and linear H_4 systems, recovering the noisy data back toward the FCI benchmark. This demonstrates that while the optimal choice of k depends on the specific hardware noise profile and the local steepness of the potential energy surface, our distance-constrained RDM framework remains a versatile and viable strategy for enhancing the precision of near-term quantum simulations.

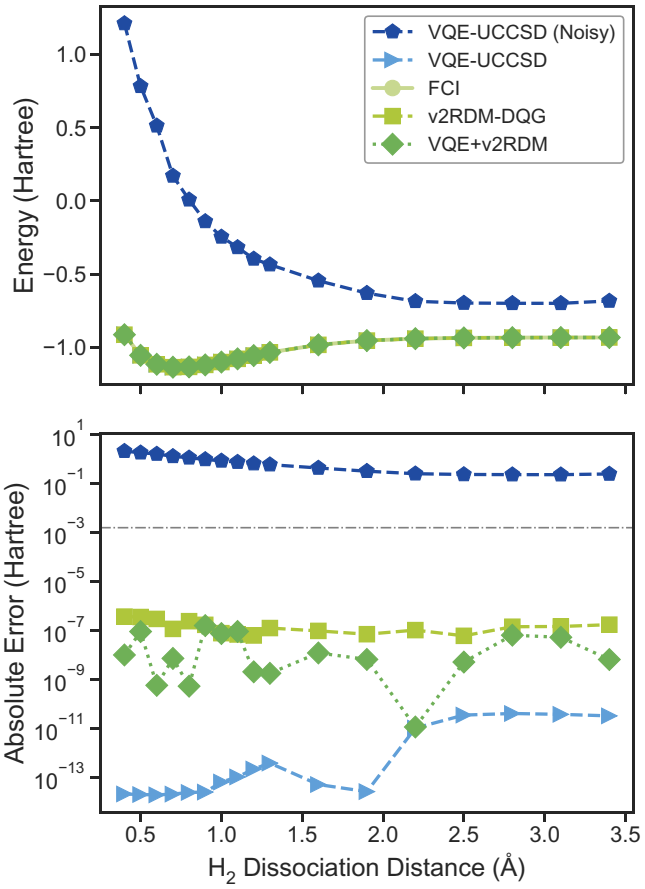

FIG. 6. Comparison of calculated absolute energy errors for H_2 under the FAKE_GUADALUPE noise model. By specifically expanding the trust radius scaling factor to $k = 3$ for short internuclear distances (< 2 Å), the anomalous energy spikes observed under the $k = 2$ setting are eliminated. In this regime, the $k = 3$ correction yields results superior to the unmitigated noisy UCCSD circuit, successfully restoring chemical accuracy.

D. Signal denoising in UED simulation

Having demonstrated the capability of our framework to correct PECs involving bond-breaking processes governed by evolving electron correlation, we now extend its application to another critical area of quantum dynamics: the simulation of experimental observables in UED [69–71]. UED is a widely used technique that directly probes atomic-scale structural dynamics during chemical reactions, such as the bond-breaking events illustrated in the previous section. However, extracting accurate structural information from UED signals requires accurate electronic structure inputs, particularly the one- and

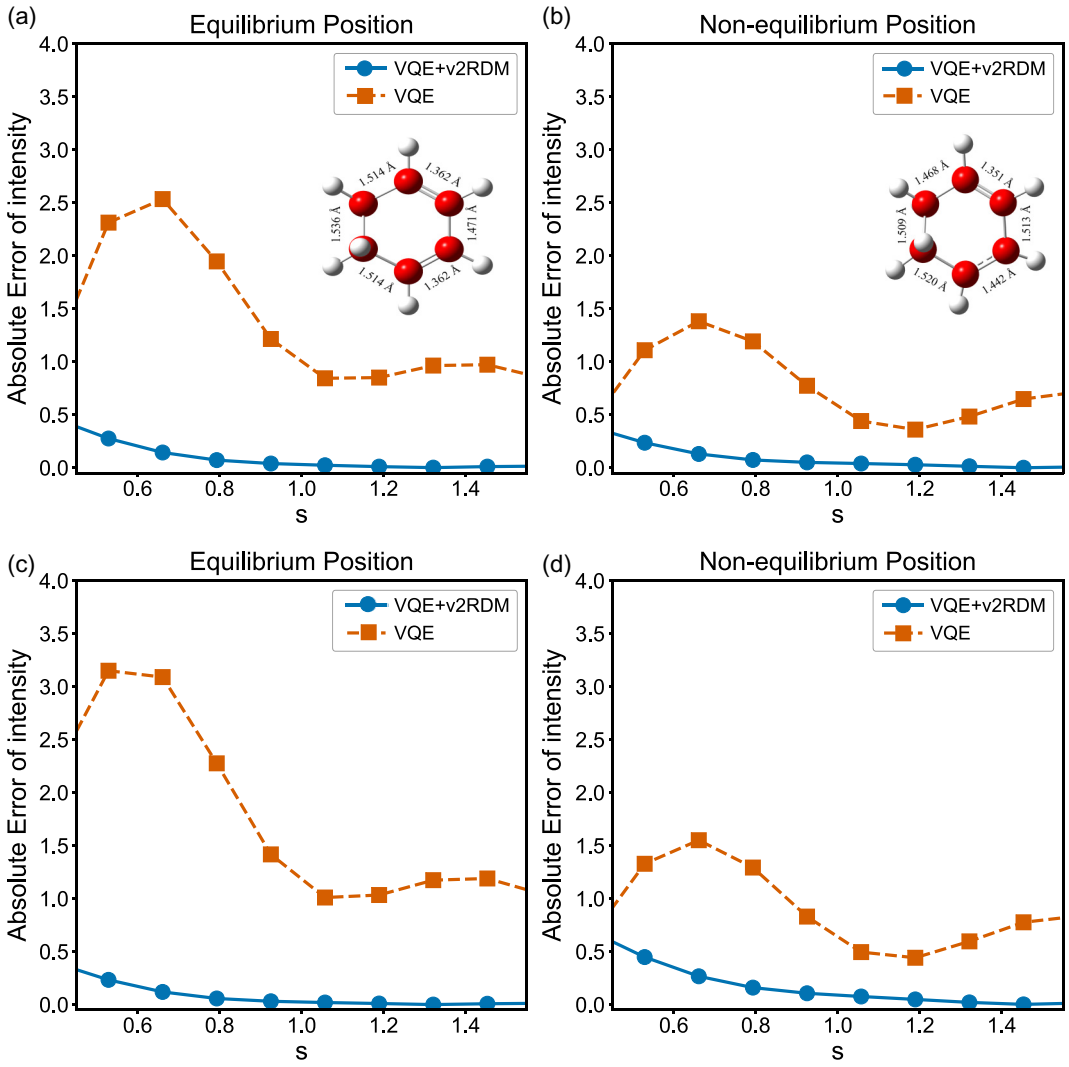

FIG. 7. Absolute error of the simulated UED intensity for the C_6H_8 molecule. Panels (a),(b) display the results evaluated with a depolarizing noise model at the equilibrium and a nonequilibrium position, respectively. Panels (c),(d) present the corresponding results simulated using an IBM fake backend at the equilibrium and a nonequilibrium position. The orange dashed line with square markers ("VQE") indicates the error of the spectrum calculated using the VQE in a noisy environment relative to the exact, noiseless solution. The blue solid line with circle markers ("VQE + v2RDM") represents the error after applying our proposed VQE plus v2RDM correction method.

two-electron RDMs, which are susceptible to noise on quantum hardware.

For a given wave function $|\psi\rangle$, the scattering intensity in UED can be simulated using the incoming electron or photon energy ϵ_0 and scattered electron or photon energy ϵ_s [72],

$$I(\vec{s},\epsilon_s,i)=\frac{\epsilon_s}{\epsilon_0}\|\langle\psi_0|\hat{L}|\psi_i\rangle\|^2\delta(E_0+\epsilon_0-E_i-\epsilon_s), \quad (10)$$

where the $\vec{s}$ is the momentum transfer vector, $\hat{L}$ is the scattering operator, and E_0 and E_i are the energies for the initial (ψ_0) and final (ψ_i) states, respectively. The signal can be expanded into elastic and inelastic components. In second-quantized form, these components can be expressed as

$$I(\vec{s},\text{elastic})=|C_{N^\alpha}|^2-2C_{N^\alpha}\sum_{ij}D^i_jS_{ij}+\sum_{ij}\sum_{kl}D^i_jD^k_lS_{i,j}S^*_{kl} \quad (11)$$

and

$$I(\vec{s},\text{inelastic})=n+\sum_{ijkl}D^{ij}_{kl}S_{ij}S^*_{kl}-\sum_{ij}\sum_{kl}D^i_jD^k_lS_{i,j}S^*_{kl}, \quad (12)$$

where S denotes diffraction integrals in the molecular orbitals basis and C_{N^α} and n are constants related to the nucleus and electrons, respectively. Interpreting UED signals requires highly accurate electron correlation models, as the scattering intensity $I(\vec{s})$ sensitively depends on the many-body electronic structure [Eqs. (11) and (12)], particularly the one- and two-electron RDMs, which are susceptible to noise on quantum hardware.

To ensure computational feasibility, we performed the C_6H_8 simulations using an active space approximation with the 6-31G basis set. Utilizing the MOKIT and PYSCF packages, we identified a complete active space (CAS) comprising 4 electrons in 4 spatial orbitals, denoted as CAS(4, 4) (indices 21–24 were active, while indices 0–20 were frozen). This setup mapped the problem to an effective eight-qubit Hamiltonian. Furthermore, to maintain consistency with the benchmarks in previous sections, the VQE simulations employed the UCCSD *Ansatz*. To comprehensively evaluate the robustness of our correction method, we conducted simulations under two distinct noise conditions: the previously used depolarizing noise model, characterized by single-qubit gate error rates of $p_1 = 0.001$ and two-qubit gate error rates of $p_2 = 0.01$, as well as a hardware-realistic noise model utilizing an IBM fake backend with the FAKE_GUADALUPE processor as illustrated in Fig. 4.

By applying the same noise-aware correction protocol, we show that our method effectively reduces noise in UED signals simulated from both noisy environments, thereby establishing a reliable and versatile quantum-classical pipeline for predicting complex experimental observables. The simulated UED signal is shown in Fig. 7, demonstrating that our purified RDMs reduce errors under both the depolarizing noise and the IBM fake backend simulations. Since the signal intensity approaches zero for small s, we restrict our analysis to the range of $s = 0.5$–1.5 to optimize computational efficiency.

V. CONCLUSION

In this work, we have established a quantum-classical framework that systematically refines the noisy outputs of quantum computers to determine ground-state properties with high precision. The method enforces N-representability conditions on the experimentally measured 2-RDM within a trust region, which is defined by a norm-based distance constraint. A practical, hardware-efficient protocol for calibrating this trust region was introduced, leveraging classically simulable Clifford circuits to establish a direct link to the hardware's noise characteristics. The efficacy and high fidelity of this approach were validated through numerical simulations on molecules including H_2, LiH, and H_4, well as by the accurate computation of the UED scattering intensity of C_6H_8.

This framework provides a methodology for simultaneously correcting hardware noise and addressing the expressive limitations of the quantum *Ansatz*. By incorporating classical constraints into the quantum computational output, the method recovers physically consistent RDMs from NISQ devices. A key strength of this framework is its generality; although our demonstrations utilized standard DQG N-representability conditions and semidefinite programming, the architecture is inherently flexible, designed to incorporate more advanced constraints and state-of-the-art algorithms from v2RDM theory [73–75]. Furthermore, the scalability of the classical postprocessing, especially when augmented with symmetry considerations, suggests a viable path toward treating systems of over 30 electrons [73]. We anticipate that this approach will be a useful tool in the efforts to utilize near-term quantum computers for scientific discovery.

ACKNOWLEDGMENTS

This work is supported by Quantum Science and Technology-National Science and Technology Major Project (2023ZD0300200), the National Natural Science Foundation of China NSAF (Grants No. U2330201 and No. 12361161602), and Beijing Natural Science Foundation (Grants No. Z250004 and No. 1254053). Y.M. acknowledges support by the National Natural Science Foundation of China (Grants No. 22173114, No. 22333003) and the Strategic Priority Research Program (Grant No. XDB0500101), Youth Innovation Promotion Association (Grant No. 2022168) of the Chinese Academy of Sciences. The scientific calculations in this paper were supported by the High-performance Computing Platform of Peking University and ORISE and ERA supercomputers of Chinese Academy of Sciences.

DATA AVAILABILITY

The data that support the findings of this article are openly available [76], embargo periods may apply.

APPENDIX: SUPPORTING INFORMATION: METHODS

In this section, we present and prove two theorems that establish theoretical bounds on the trust radius Δ. To formalize this, we first define the error, Δ, as the Frobenius norm of the difference between the ideal RDM from a state ρ and the experimentally measured noisy RDM.

Definition A1. Let $(D^{pq}_{rs})_{\text{ideal}}$ denote the ideal 2-RDM resulting from a quantum state ρ and let $(D^{pq}_{rs})_{\text{noisy}}$ represent the 2-RDM obtained from measurements performed on a quantum device. The error Δ between the ideal and

noisy measurements is defined as

$$\Delta(\rho) \equiv \sqrt{\sum_{rspq} \left[(D_{rs}^{pq})_{\text{ideal}} - (D_{rs}^{pq})_{\text{noisy}} \right]^2}. \tag{A1}$$

Our first theorem establishes a bound on this error based on a local depolarizing noise model, where each gate contributes independently to the total error.

Theorem A1. Let a quantum circuit consist of n qubits, with n_1 single-qubit gates and n_2 two-qubit gates. Assume the presence of local depolarizing noise in the circuit, with error probabilities p_{k_1} for single-qubit gates and p_{k_2} for two-qubit gates. Let ρ denote the quantum state corresponding to the ideal circuit. Then, the error $\Delta(\rho)$ between the ideal and noisy measurements satisfies a bound

$$\Delta(\rho) \leq 2n^2 \sum_{k_1,k_2}^{n_1,n_2} (p_{k_1} + p_{k_2}). \tag{A2}$$

While Theorem A1 provides a general upper bound, its dependence on the sum of all individual gate errors can be loose. To derive a more structured and potentially tighter bound that depends on the circuit's depth, we now introduce a global noise model.

Definition A2. Define a global depolarizing noise model as follows: after each layer of single-qubit and two-qubit gates, the entire quantum state undergoes the following channel

$$\Phi_i(\rho) = \left(1 - p_{i_k}\right) U_i \rho U_i^\dagger + p_{i_k} \frac{I_n}{2^n}, \tag{A3}$$

where $k = 1, 2$ represents the cases for single- and two-qubit gates, respectively. Here, p_{i_k} is the corresponding error probability, U_i represents a layer of certain gates, and ρ is the original n-qubit state.

Operating under this layer-by-layer noise model, we can arrive at our second theorem, which provides an exact expression for the error.

Theorem A2. Let a quantum circuit consist of n qubits, with d_1 layers of single-qubit gates and d_2 layers of two-qubit gates. Assume the presence of a global depolarizing noise in the circuit, with error probabilities p_1 for single-qubit gates and p_2 for two-qubit gates. Let ρ denote the quantum state corresponding to the ideal circuit. Then, the error $\Delta(\rho)$ between the ideal and noisy measurements satisfies

$$\Delta(\rho) = \left[1 - (1-p_1)^{d_1} (1-p_2)^{d_2}\right] \times \sqrt{\sum_{pqrs} \left[\text{Tr}(\rho a_p^\dagger a_q^\dagger a_r a_s) - \frac{1}{2^n} \text{Tr}(a_p^\dagger a_q^\dagger a_r a_s) \right]^2}, \tag{A4}$$

where $a_i^\dagger$ and a_i represent the creation and annihilation operators for the ith qubit, respectively.

The proof of Theorem A1 is as follows.

Proof. By definition, we can write the ideal single-qubit gate as

$$\Omega_i^k(\rho_0) = U_i \rho_0 U_i^\dagger, \tag{A5}$$

representing the ith gate on kth qubit. Then, the depolarizing-noise-affected single-qubit gate channel can be written as

$$\Lambda_i^k(\rho_0) = \left(1 - p_{k_1}\right) U_i \rho_0 U_i^\dagger + p_{k_1}/2 \, \text{Tr}_k(\rho_0) \otimes I. \tag{A6}$$

The two-qubit gate situation is similar.

$$\Delta(\rho) = \sqrt{\sum_{pqrs} \left[\text{Tr}\left(\rho' a_p^\dagger a_q^\dagger a_r a_s\right) - \text{Tr}\left(\rho_1 a_p^\dagger a_q^\dagger a_r a_s\right) \right]^2}, \tag{A7}$$

where we define

$$\rho' = \Lambda_N \ldots \Lambda_1(\rho_0) \tag{A8}$$

and

$$\rho_k = \Omega_N \ldots \Omega_k \Lambda_{k-1} \ldots \Lambda_1(\rho_0). \tag{A9}$$

Since

$$\begin{aligned} &\text{Tr}\left[\Lambda(\rho) a_p^\dagger a_q^\dagger a_r a_s\right] - \text{Tr}\left[\Omega(\rho) a_p^\dagger a_q^\dagger a_r a_s\right] \\ &= \text{Tr}\left\{ p_k \left[\text{Tr}_k(\rho) \otimes I/2 - U_i \rho U_i^\dagger \right] a_p^\dagger a_q^\dagger a_r a_s \right\} \\ &\leqslant 2p_k, \quad k = 1, 2, \end{aligned} \tag{A10}$$

we can bound the summation term in Eq. (A7) to be

$$\begin{aligned} &\text{Tr}\left(\rho' a_p^\dagger a_q^\dagger a_r a_s\right) - \text{Tr}\left(\rho_1 a_p^\dagger a_q^\dagger a_r a_s\right) \\ &= \text{Tr}\left(\rho' a_p^\dagger a_q^\dagger a_r a_s\right) - \text{Tr}\left(\rho_N a_p^\dagger a_q^\dagger a_r a_s\right) + \cdots \\ &\quad + \text{Tr}\left(\rho_2 a_p^\dagger a_q^\dagger a_r a_s\right) - \text{Tr}\left(\rho_1 a_p^\dagger a_q^\dagger a_r a_s\right) \\ &\leqslant 2 \sum_{k_1,k_2}^{n_1,n_2} (p_{k_1} + p_{k_2}). \end{aligned} \tag{A11}$$

Thus,

$$\Delta(\rho) \leqslant 2n^2 \sum_{k_1,k_2}^{n_1,n_2} (p_{k_1} + p_{k_2}). \tag{A12}$$

■

The proof of Theorem A2 is as follows.

Proof. By definition, one layer of single-qubit gates of a weakened depolarizing noise channel can be written as

$$\rho_1 = \Phi_1\left(\rho_0'\right) = \left(1 - p_{k_1}\right) U_1 \rho_0 U_1^\dagger + p_{k_1} \frac{I_n}{2^n}. \tag{A13}$$

The effect of imposing a second layer of channels on top of this is given by

$$\begin{aligned} \rho_2 &= \Phi_2\left(\rho_1\right) = \left(1 - p_{k_2}\right) \rho_1 + p_{k_2} \frac{I_n}{2^n} \\ &= \left(1 - p_{k_1}\right)\left(1 - p_{k_2}\right) U_2 U_1 \rho_0 U_1^\dagger U_2^\dagger \\ &\quad + \left[\left(1 - p_{k_2}\right) p_{k_1} + p_{k_2}\right] \frac{I_n}{2^n}. \end{aligned} \tag{A14}$$

After which it becomes

$$\begin{aligned} \rho' &= (1 - p_1)^{d_1} (1 - p_2)^{d_2} U \rho_0 U^\dagger \\ &\quad + \left[1 - (1 - p_1)^{d_1} (1 - p_2)^{d_2}\right] \frac{I_n}{2^n}, \end{aligned} \tag{A15}$$

where $U = \prod_i U_i$. The ideal case is

$$\rho = U \rho_0 U^\dagger. \tag{A16}$$

Eventually, by definition of the error, we have

$$\begin{aligned} \Delta(\rho) &= \left[1 - (1 - p_1)^{d_1} (1 - p_2)^{d_2}\right] \\ &\quad \times \sqrt{\sum_{pqrs} \left[\mathrm{Tr}(\rho a_p^\dagger a_q^\dagger a_r a_s) - \frac{1}{2^n} \mathrm{Tr}(a_p^\dagger a_q^\dagger a_r a_s)\right]^2}. \end{aligned} \tag{A17}$$

■

[1] J. Wang, J. Surace, I. Frérot, B. Legat, M.-O. Renou, V. Magron, and A. Acín, Certifying ground-state properties of many-body systems, Phys. Rev. X **14**, 031006 (2024).

[2] S. R. White, Density matrix formulation for quantum renormalization groups, Phys. Rev. Lett. **69**, 2863 (1992).

[3] M. Reiher, N. Wiebe, K. M. Svore, D. Wecker, and M. Troyer, Elucidating reaction mechanisms on quantum computers, Proc. Natl. Acad. Sci. **114**, 7555 (2017).

[4] P. A. Lee, N. Nagaosa, and X.-G. Wen, Doping a Mott insulator: Physics of high-temperature superconductivity, Rev. Mod. Phys. **78**, 17 (2006).

[5] J. Rayleigh, In finding the correction for the open end of an organ-pipe, Phil. Trans **161**, 16 (1870).

[6] J. K. L. MacDonald, Successive approximations by the Rayleigh-Ritz variation method, Phys. Rev. **43**, 830 (1933).

[7] A. Peruzzo, J. McClean, P. Shadbolt, M.-H. Yung, X.-Q. Zhou, P. J. Love, A. Aspuru-Guzik, and J. L. O'brien, A variational eigenvalue solver on a photonic quantum processor, Nat. Commun. **5**, 4213 (2014).

[8] J. R. McClean, J. Romero, R. Babbush, and A. Aspuru-Guzik, The theory of variational hybrid quantum-classical algorithms, New J. Phys. **18**, 023023 (2016).

[9] M. Cerezo, A. Arrasmith, R. Babbush, S. C. Benjamin, S. Endo, K. Fujii, J. R. McClean, K. Mitarai, X. Yuan, L. Cincio, and P. J. Coles, Variational quantum algorithms, Nat. Rev. Phys. **3**, 625 (2021).

[10] J. Tilly, H. Chen, S. Cao, D. Picozzi, K. Setia, Y. Li, E. Grant, L. Wossnig, I. Rungger, G. H. Booth, and J. Tennyson, The variational quantum eigensolver: A review of methods and best practices, Phys. Rep. **986**, 1 (2022).

[11] A. Kandala, A. Mezzacapo, K. Temme, M. Takita, M. Brink, J. M. Chow, and J. M. Gambetta, Hardware-efficient variational quantum eigensolver for small molecules and quantum magnets, Nature **549**, 242 (2017).

[12] A. Kandala, K. Temme, A. D. Córcoles, A. Mezzacapo, J. M. Chow, and J. M. Gambetta, Error mitigation extends the computational reach of a noisy quantum processor, Nature **567**, 491 (2019).

[13] S. Guo, J. Sun, H. Qian, M. Gong, Y. Zhang, F. Chen, Y. Ye, Y. Wu, S. Cao, K. Liu *et al.*, Experimental quantum computational chemistry with optimized unitary coupled cluster ansatz, Nat. Phys. **20**, 1240 (2024).

[14] Y. Ma, W. Wang, X. Mu, W. Cai, Z. Hua, X. Pan, D.-L. Deng, R. Wu, C.-L. Zou, L. Wang *et al.*, Experimental implementation of a qubit-efficient variational quantum eigensolver with analog error mitigation on a superconducting quantum processor, Sci. China Phys., Mech. Astron. **68**, 270311 (2025).

[15] F. Arute *et al.* (G. A. Quantum, Collaborators*†), Hartree-Fock on a superconducting qubit quantum computer, Science **369**, 1084 (2020).

[16] J. Preskill, Quantum computing in the NISQ era and beyond, Quantum **2**, 79 (2018).

[17] S. Endo, Z. Cai, S. C. Benjamin, and X. Yuan, Hybrid quantum-classical algorithms and quantum error mitigation, J. Phys. Soc. Jpn. **90**, 032001 (2021).

[18] Z. Cai, R. Babbush, S. C. Benjamin, S. Endo, W. J. Huggins, Y. Li, J. R. McClean, and T. E. O'Brien, Quantum error mitigation, Rev. Mod. Phys. **95**, 045005 (2023).

[19] S. Endo, S. C. Benjamin, and Y. Li, Practical quantum error mitigation for near-future applications, Phys. Rev. X **8**, 031027 (2018).

[20] A. J. Coleman, Structure of fermion density matrices, Rev. Mod. Phys. **35**, 668 (1963).

[21] M. Nakata, H. Nakatsuji, M. Ehara, M. Fukuda, K. Nakata, and K. Fujisawa, Variational calculations of fermion second-order reduced density matrices by semidefinite programming algorithm, J. Chem. Phys. **114**, 8282 (2001).

[22] D. A. Mazziotti, Variational minimization of atomic and molecular ground-state energies via the two-particle reduced density matrix, Phys. Rev. A **65**, 062511 (2002).
[23] D. A. Mazziotti, Two-electron reduced density matrix as the basic variable in many-electron quantum chemistry and physics, Chem. Rev. **112**, 244 (2012).
[24] X. Bonet-Monroig, R. Babbush, and T. E. O'Brien, Nearly optimal measurement scheduling for partial tomography of quantum states, Phys. Rev. X **10**, 031064 (2020).
[25] W. Ritz, Über eine neue methode zur lösung gewisser variationsprobleme der mathematischen physik., J. Reine Angew. Math. **1909**, 1 (1909).
[26] C. Garrod and J. K. Percus, Reduction of the N-particle variational problem, J. Math. Phys. **5**, 1756 (1964).
[27] C. Garrod, M. V. Mihailović, and M. Rosina, The variational approach to the two body density matrix, J. Math. Phys. **16**, 868 (1975).
[28] R. M. Erdahl, Representability, Int. J. Quantum Chem. **13**, 697 (1978).
[29] R. M. Erdahl, C. Garrod, B. Golli, and M. Rosina, The application of group theory to generate new representability conditions for rotationally invariant density matrices, J. Math. Phys. **20**, 1366 (1979).
[30] P.-O. Löwdin, Quantum theory of many-particle systems. I. Physical interpretations by means of density matrices, natural spin-orbitals, and convergence problems in the method of configurational interaction, Phys. Rev. **97**, 1474 (1955).
[31] J. E. Mayer, Electron correlation, Phys. Rev. **100**, 1579 (1955).
[32] R. H. Tredgold, Density matrix and the many-body problem, Phys. Rev. **105**, 1421 (1957).
[33] G. Gidofalvi and D. A. Mazziotti, Active-space two-electron reduced-density-matrix method: Complete active-space calculations without diagonalization of the N-electron Hamiltonian, J. Chem. Phys. **129**, 134108 (2008).
[34] A. V. Sinitskiy, L. Greenman, and D. A. Mazziotti, Strong correlation in hydrogen chains and lattices using the variational two-electron reduced density matrix method, J. Chem. Phys. **133**, 014104 (2010).
[35] I. DePrince, A. Eugene, and D. A. Mazziotti, Exploiting the spatial locality of electron correlation within the parametric two-electron reduced-density-matrix method, J. Chem. Phys. **132**, 034110 (2010).
[36] I. DePrince, A. Eugene, and D. A. Mazziotti, Isomerization of nitrosomethane to formaldoxime: Energies, geometries, and frequencies from the parametric variational two-electron reduced-density-matrix method, J. Chem. Phys. **133**, 034112 (2010).
[37] G. Gidofalvi and D. A. Mazziotti, Computation of quantum phase transitions by reduced-density-matrix mechanics, Phys. Rev. A **74**, 012501 (2006).
[38] C. A. Schwerdtfeger and D. A. Mazziotti, Convex-set description of quantum phase transitions in the transverse Ising model using reduced-density-matrix theory, J. Chem. Phys. **130**, 224102 (2009).
[39] E. Kamarchik and D. A. Mazziotti, Variational reduced-density-matrix method for ground-state nuclear motion, Phys. Rev. A **75**, 013203 (2007).
[40] E. Kamarchik and D. A. Mazziotti, Coupled nuclear and electronic ground-state motion from variational reduced-density-matrix theory with applications to molecules with floppy or resonant hydrogens, Phys. Rev. A **79**, 012502 (2009).
[41] E. Kamarchik and D. A. Mazziotti, Global energy minima of molecular clusters computed in polynomial time with semidefinite programming, Phys. Rev. Lett. **99**, 243002 (2007).
[42] D. A. Mazziotti, Large-scale semidefinite programming for many-electron quantum mechanics, Phys. Rev. Lett. **106**, 083001 (2011).
[43] J. E. Subotnik, T. Hansen, M. A. Ratner, and A. Nitzan, Nonequilibrium steady state transport via the reduced density matrix operator, J. Chem. Phys. **130**, 144105 (2009).
[44] A. E. Rothman and D. A. Mazziotti, Nonequilibrium, steady-state electron transport with N-representable density matrices from the anti-Hermitian contracted Schrödinger equation, J. Chem. Phys. **132**, 104112 (2010).
[45] J. C. Phillips, Percolative theories of strongly disordered ceramic high-temperature superconductors, Proc. Natl. Acad. Sci. **107**, 1307 (2010).
[46] N. C. Rubin, R. Babbush, and J. McClean, Application of fermionic marginal constraints to hybrid quantum algorithms, New J. Phys. **20**, 053020 (2018).
[47] C. Lanssens, P. W. Ayers, D. Van Neck, S. De Baerdemacker, K. Gunst, and P. Bultinck, Method for making 2-electron response reduced density matrices approximately N-representable, J. Chem. Phys. **148**, 084104 (2018).
[48] T. Piskor, F. G. Eich, M. Marthaler, F. K. Wilhelm, and J.-M. Reiner, Post-processing noisy quantum computations utilizing N-representability constraints, arXiv:2304.13401.
[49] D. A. Mazziotti, Quantum many-body theory from a solution of the N-representability problem, Phys. Rev. Lett. **130**, 153001 (2023).
[50] I. Avdic and D. A. Mazziotti, Fewer measurements from shadow tomography with N-representability conditions, Phys. Rev. Lett. **132**, 220802 (2024).
[51] G.-L. R. Anselmetti, M. Degroote, N. Moll, R. Santagati, and M. Streif, Classical optimisation of reduced density matrix estimations with classical shadows using N-representability conditions under shot noise considerations, arXiv:2411.18430.
[52] Y.-K. Liu, M. Christandl, and F. Verstraete, Quantum computational complexity of the N-representability problem: QMA complete, Phys. Rev. Lett. **98**, 110503 (2007).
[53] Z. Zhao, B. J. Braams, M. Fukuda, M. L. Overton, and J. K. Percus, The reduced density matrix method for electronic structure calculations and the role of three-index representability conditions, J. Chem. Phys. **120**, 2095 (2004).
[54] S. E. Smart and D. A. Mazziotti, Quantum-classical hybrid algorithm using an error-mitigating N-representability condition to compute the Mott metal-insulator transition, Phys. Rev. A **100**, 022517 (2019).
[55] M. Urbanek, B. Nachman, V. R. Pascuzzi, A. He, C. W. Bauer, and W. A. de Jong, Mitigating depolarizing noise on quantum computers with noise-estimation circuits, Phys. Rev. Lett. **127**, 270502 (2021).

[56] R. C. Farrell, M. Illa, A. N. Ciavarella, and M. J. Savage, Scalable circuits for preparing ground states on digital quantum computers: The Schwinger model vacuum on 100 qubits, PRX Quantum **5**, 020315 (2024).

[57] D. Gottesman, in *Group22: Proceedings of the XXII International Colloquium on Group Theoretical Methods in Physics*, edited by S. P. Corney, R. Delbourgo, and P. D. Jarvis (International Press, Cambridge, MA, 1999), pp. 32–43.

[58] P. K. Barkoutsos, J. F. Gonthier, I. Sokolov, N. Moll, G. Salis, A. Fuhrer, M. Ganzhorn, D. J. Egger, M. Troyer, A. Mezzacapo, S. Filipp, and I. Tavernelli, Quantum algorithms for electronic structure calculations: Particle-hole Hamiltonian and optimized wave-function expansions, Phys. Rev. A **98**, 022322 (2018).

[59] Q. Sun, T. C. Berkelbach, N. S. Blunt, G. H. Booth, S. Guo, Z. Li, J. Liu, J. D. McClain, E. R. Sayfutyarova, S. Sharma, S. Wouters, and G. K.-L. Chan, PySCF: The Python-based simulations of chemistry framework, WIREs Comput. Mol. Sci. **8**, e1340 (2018).

[60] Q. Sun *et al.*, Recent developments in the PySCF program package, J. Chem. Phys. **153**, 024109 (2020).

[61] H. R. Grimsley, S. E. Economou, E. Barnes, and N. J. Mayhall, An adaptive variational algorithm for exact molecular simulations on a quantum computer, Nat. Commun. **10**, 3007 (2019).

[62] J. T. Seeley, M. J. Richard, and P. J. Love, The Bravyi–Kitaev transformation for quantum computation of electronic structure, J. Chem. Phys. **137**, 224109 (2012).

[63] M. Ganzhorn, D. Egger, P. Barkoutsos, P. Ollitrault, G. Salis, N. Moll, M. Roth, A. Fuhrer, P. Mueller, S. Woerner, I. Tavernelli, and S. Filipp, Gate-efficient simulation of molecular eigenstates on a quantum computer, Phys. Rev. Appl. **11**, 044092 (2019).

[64] D. Singh, S. Mehendale, Arvind, and K. Dorai, Ground and excited state energy calculations of the H_2 molecule using a variational quantum eigensolver algorithm on an NMR quantum simulator, arXiv preprint arXiv:2407.01000.

[65] R. H. Byrd, P. Lu, J. Nocedal, and C. Zhu, A limited memory algorithm for bound constrained optimization, SIAM J. Sci. Comput. **16**, 1190 (1995).

[66] M. J. Powell, in *Advances in Optimization and Numerical Analysis* (Springer, Dordrecht, Netherlands, 1994), pp. 51–67.

[67] J. Spall, Multivariate stochastic approximation using a simultaneous perturbation gradient approximation, IEEE Trans. Automat. Contr. **37**, 332 (1992).

[68] S. Diamond and S. Boyd, CVXPY: A Python-embedded modeling language for convex optimization, J. Mach. Learn. Res. **17**, 1 (2016).

[69] M. Centurion, T. J. Wolf, and J. Yang, Ultrafast imaging of molecules with electron diffraction, Annu. Rev. Phys. Chem. **73**, 21 (2022).

[70] D. Filippetto, P. Musumeci, R. K. Li, B. J. Siwick, M. R. Otto, M. Centurion, and J. P. F. Nunes, Ultrafast electron diffraction: Visualizing dynamic states of matter, Rev. Mod. Phys. **94**, 045004 (2022).

[71] E. G. Champenois *et al.*, Femtosecond electronic and hydrogen structural dynamics in ammonia imaged with ultrafast electron diffraction, Phys. Rev. Lett. **131**, 143001 (2023).

[72] J. Yang, X. Zhu, J. P. F. Nunes, J. K. Yu, R. M. Parrish, T. J. Wolf, M. Centurion, M. Gühr, R. Li, Y. Liu *et al.*, Simultaneous observation of nuclear and electronic dynamics by ultrafast electron diffraction, Science **368**, 885 (2020).

[73] D. A. Mazziotti, Enhanced constraints for accurate lower bounds on many-electron quantum energies from variational two-electron reduced density matrix theory, Phys. Rev. Lett. **117**, 153001 (2016).

[74] J. Fosso-Tande, T.-S. Nguyen, G. Gidofalvi, and A. E. DePrince III, Large-scale variational two-electron reduced-density-matrix-driven complete active space self-consistent field methods, J. Chem. Theory Comput. **12**, 2260 (2016).

[75] D. A. Mazziotti, Dual-cone variational calculation of the two-electron reduced density matrix, Phys. Rev. A **102**, 052819 (2020).

[76] Q.-M. Ding, J. Peng, J. Huang, Y. Zhang, H. Wang, X. Xu, J. Ren, Y. Ma, and X. Yuan, Data and code for the manuscript, https://doi.org/10.5281/zenodo.19157208 (2026).